OPEN

The Novel MyD88 Inhibitor TJ-M2010-5 Protects Against Hepatic Ischemia-reperfusion Injury by Suppressing Pyroptosis in Mice

Zhimiao Zou, MD,[1,2,3,4] Runshi Shang, MS,[1,2,3,4] Liang Zhou, MS,[1,2,3,4] Dunfeng Du, PhD,[1,2,3,4] Yang Yang, MD,[1,2,3,4] Yalong Xie, MD,[1,2,3,4] Zeyang Li, MD,[1,2,3,4] Minghui Zhao, MS,[1,2,3,4] Fengchao Jiang, PhD,[5] Limin Zhang, PhD,[1,2,3,4] and Ping Zhou, PhD[1,2,3,4]

Background. With the development of medical technology and increased surgical experience, the number of patients receiving liver transplants has increased. However, restoration of liver function in patients is limited by the occurrence of hepatic ischemia-reperfusion injury (IRI). Previous studies have reported that the Toll-like receptor 4 (TLR4)/myeloid differentiation factor 88 (MyD88) signaling pathway and pyroptosis play critical roles in the development of hepatic IRI. **Methods**. A mouse model of segmental (70%) warm hepatic IRI was established using BALB/c mice in vivo. The mechanism underlying inflammation in mouse models of hepatic IRI was explored in vitro using lipopolysaccharide- and ATP-treated bone marrow-derived macrophages. This in vitro inflammation model was used to simulate inflammation and pyroptosis in hepatic IRI. **Results**. We found that a MyD88 inhibitor conferred protection against partial warm hepatic IRI in mouse models by downregulating the TLR4/MyD88 signaling pathway. Moreover, TJ-M2010-5 (a novel MyD88 inhibitor, hereafter named TJ-5) reduced hepatic macrophage depletion and pyroptosis induction by hepatic IRI. TJ-5 treatment inhibited pyroptosis in bone marrow-derived macrophages by reducing the nuclear translocation of nuclear factor kappa-light-chain-enhancer of activated B cells, decreasing the release of high-mobility group box-1, and promoting endocytosis of lipopolysaccharide-high-mobility group box-1 complexes. **Conclusions**. Inhibition of MyD88 may protect the liver from partial warm hepatic IRI by reducing pyroptosis in hepatic innate immune cells. These results reveal the mechanism underlying the development of inflammation in partially warm hepatic IRI and the induction of cell pyroptosis.

(*Transplantation* 2023;107: 392–404).

INTRODUCTION

Hepatic ischemia-reperfusion injury (IRI) is unavoidable during liver transplantation and partial hepatectomy and may cause multiple organ failures.[1] Hepatic IRI entails direct hepatocyte injury caused by ischemia and an inflammatory cascade triggered by inflammatory pathway activation during perfusion.[2] Toll-like receptors (TLRs) on the Kupffer cell surface are activated by endogenous damage-associated molecular patterns, which provide the trigger pro-inflammatory responses.[3,4] TLRs, mostly Toll-like receptor 4 (TLR4),[4] in hepatic macrophages rely on myeloid differentiation factor 88 (MyD88) to trigger downstream signaling.[2,5] Notably, activation of the TLR4/MyD88 signaling pathway in liver macrophages plays a key role in the development of inflammation in hepatic IRI, a phenomenon that leads to severe liver damage.

Received 11 April 2022. Revision received 17 June 2022.

Accepted 21 June 2022.

[1] *Institute of Organ Transplantation, Tongji Hospital, Tongji Medical College, Huazhong University of Science and Technology, Wuhan, Hubei, China.*

[2] *Key Laboratory of Organ Transplantation, Ministry of Education, Wuhan, Hubei, China.*

[3] *NHC Key Laboratory of Organ Transplantation, Wuhan, Hubei, China.*

[4] *Key Laboratory of Organ Transplantation, Chinese Academy of Medical Sciences, Wuhan, Hubei, China.*

[5] *Academy of Pharmacy, Tongji Medical College, Huazhong University of Science and Technology, Wuhan, Hubei, China.*

This work was supported by the National Natural Science Foundation of China (No. 81974017).

The authors declare no conflicts of interest.

Z.Z. conceived the study, conducted the experiments and data analysis, established the models, and wrote the article. R.S. assisted in modeling and sample collection. L.Zho. assisted with data interpretation and mapping. D.D. revised the article. Y.Y. and Y.X. contributed to the experimental design. Z.L. participated in the data interpretation. M.Z. contributed to the sample collection. F.J. synthesized TJ-5. L.Zha. conceived and supervised the research and revised the article. P.Z. conceived the study, designed the experiments, and supervised the research.

Supplemental digital content (SDC) is available for this article. Direct URL citations appear in the printed text, and links to the digital files are provided in the HTML text of this article on the journal's Web site (www.transplantjournal.com).

Correspondence: Limin Zhang, PhD, Institute of Organ Transplantation, Tongji Hospital, Tongji Medical College, Huazhong University of Science and Technology, 1095 Jiefang Road, Wuhan, Hubei 430030, China. (zhanglimingq@126.com); or Ping Zhou, PhD, Institute of Organ Transplantation, Tongji Hospital, Tongji Medical College, Huazhong University of Science and Technology, 1095 Jiefang Road, Wuhan, Hubei 430030, China. (pzhou@tjh.tjmu.edu.cn).

ISSN: 0041-1337/20/1072-392

DOI: 10.1097/TP.0000000000004317

Researchers have recently identified a novel form of programmed cell death, termed pyroptosis, which occurs exclusively in myeloid innate immune cells but not in hepatocytes during hepatic IRI.[6] The experimental results demonstrated that pyroptosis can exacerbate hepatic injury in a mouse model of hepatic IRI,[6-9] suggesting that it plays a key role in hepatic IRI. Numerous studies have proposed that nucleotide-binding oligomerization domain-like receptors family pyrin domain containing 3 (NLRP3) can be activated by the TLR4/MyD88/nuclear factor kappa-light-chain-enhancer of activated B cells (NF-κB) signaling pathway.[10,11] Notably, the NLRP3 inflammasome complex activated caspase-1 cleaves gasdermin D (GSDMD) to the GSDMD-N terminus, thereby creating pores in the plasma membrane.[12] These membrane pores subsequently cause cell swelling and membrane rupture, thereby releasing vast amounts of inflammatory factors, such as interleukin (IL)-1β and IL-18,[12] a process termed canonical or caspase-1-dependent pyroptosis.

Lipopolysaccharide (LPS) can directly bind caspase-11 to trigger noncanonical or caspase-11-dependent pyroptosis.[13] Caspase-11-dependent pyroptosis also involves cellular membrane pore formation, cell swelling, and membrane rupture, phenomena that cause massive leakage of inflammatory cytokines.[12] NLRP3 activation requires MyD88-mediated activation of NF-κB signaling to trigger canonical pyroptosis.[10,14] Recent studies have suggested that LPS forms complexes with high-mobility group box-1 (HMGB1).[10] Notably, the LPS-HMGB1 complex is subsequently transported into the cytosol of macrophages via the receptor for advanced glycation end products (RAGE).[15] Coincidentally, RAGE requires MyD88 to initiate its downstream signaling,[16] suggesting that MyD88 is an important signaling pathway in both canonical and noncanonical pyroptosis.

Therefore, we designed and synthesized MyD88 inhibitors, termed TJ-M2010s (WIPO patent application number: PCT/CN2012/070811).[17] It had been confirmed that the TJ-M2010-5 (TJ-5) (one of the TJ-M2010s) promoted robust allograft tolerance in mouse cardiac and skin transplantation in our previous research.[18] In this study, we established a nonlethal segmental (70%) partial warm liver IRI mouse model that caused acute liver failure[19,20] to evaluate the efficacy of TJ-5. The mechanism underlying inflammation in mouse models of hepatic IRI was explored in vitro using LPS- and ATP-treated bone marrow-derived macrophages (BMDMs). We explored whether the protective effects of TJ-5 on hepatic IRI are mediated via suppressing pyroptosis.

MATERIALS AND METHODS

Animals

Six to 8-wk-old male BALB/c wild-type mice were obtained from the Experimental Animal Tech Co of Weitonglihua (Beijing, China) and maintained in the Laboratory Animal Center of Scientific Research Building, Tongji Hospital, Tongji Medical College, Huazhong University of Science and Technology. All animal experiments were approved by the Ethics of Committees of Tongji Hospital, Tongji Medical College, Huazhong University of Science and Technology, and all procedures were performed following the relevant guidelines and regulations of the Chinese Council on Animal Care.

Hepatic IRI and Treatment

Segmental (70%) hepatic warm ischemia-reperfusion mouse models were established as previously reported.[21] For surgery, the mice were anesthetized using isoflurane (4% isoflurane for induction and 1.5% isoflurane for maintenance). Mice in the control group (sham) had exposed hepatic portal veins and did not include obstructed blood flow, whereas the hepatic IRI group (IRI) had a blocked blood supply to the left lobe and mid-hepatic lobe for 60 min, followed by 6 h reperfusion. All mice were given postoperative analgesia carprofen (5 mg/kg) and maintained at 35–37 °C in warming boxes. All procedures were performed in the same laboratory by the same operator. TJ-5 was intraperitoneally administered for 3 consecutive days (called preventive administration) before liver ischemia and was used as the administration group (IRI + TJ-5). Two hours after the final administration in the IRI + TJ-5 group, all mice were subjected to surgery. For mice in the sham group, an equal volume of double-distilled water (the solvent used for TJ-5) was administered in the same manner. All mice were handled with great care to avoid puncturing their organs. But, still 2 mice in each of the IRI group and the IRI + TJ-5 group dead before the end of reperfusion assays because of operational errors. Samples were discarded if the mice did not survive before the end of reperfusion assays. Blood and liver samples were obtained under sterile conditions. The left lateral lobe of the liver was used for histological analysis, whereas the middle lobe of the liver was used for protein/RNA extraction.

Biochemical and Enzyme-linked Immunoassays

Mice were anesthetized, and blood samples were obtained by removing the eyeballs. Blood samples were centrifuged at 3000 rpm for 15 min to obtain supernatants. Serum hepatic enzyme levels were measured using an Automatic Biochemical Analyzer (Mindray). The expression of various inflammatory factors and HMGB1 in serum or supernatants from cell culture samples was measured using Enzyme-linked Immunoassays kits (Dakewe Biological Technology Co Ltd, Shenzhen, China, and Cloud-Clone Corp, Wuhan, China), according to the manufacturer's instructions.

Histological Analysis, Immunohistochemistry, and Immunofluorescence Staining

Liver tissue sections were stained with hematoxylin and eosin, and liver injury was evaluated using Suzuki's score criteria.[22] The terminal deoxynucleotidyltransferase-mediated dUTP nick-end labeling assay (Servicebio, Wuhan, China) was performed to detect hepatocyte apoptosis in each group, as instructed by the manufacturer. Immunohistochemistry (IHC) and immunofluorescence (IF) staining of the liver tissue samples were performed as reported previously.[23] The anti-F4/80 rabbit (1:200 for IF), anti-myeloperoxidase (MPO) rabbit (1:500 for IHC), and anti-CD11b rabbit (1:500 for IHC) antibodies were purchased from Servicebio (Wuhan, China). All histological slides were 4-um thick. For IF staining of BMDMs, all cells were cultured on 35-mm glass-bottom dishes. Primary detection antibodies for HMGB1 (1:200 dilution, Cloud-Clone Corp) and MyD88 (1:200 dilution, ABclonal) were added to the samples. The following day (day 2), the samples were incubated with the secondary antibody (1:200 dilution; Cy3 labeled, ABclonal,

Wuhan, China) for 30 min. Hoechst 33342 (Invitrogen) was incubated with the cells for 5 min. Finally, the cells were imaged using a confocal imaging system (UltraVIEW Vox; PerkinElmer). Three to 6 images from random fields were obtained for each stained section and at least 3 samples per group were used for each experiment. Image-Pro Plus 6.0 was used to analyze all images. Manders coefficient and Pearson coefficient were determined using the Just Another Colocalization Plugin (JACoP) plug-in of ImageJ.

BMDM Isolation, Culture, and Treatment

The tibiofibular bones were obtained from 6- to 8-wk-old male BALB/c mice. Bone marrow was lysed in a red blood cell lysis buffer (Beyotime, Shanghai, China) on ice for 5 min. The samples were subsequently cultured in 6-well plates (1×10^6 cells/mL) containing DMEM supplemented with 10% fetal bovine serum (HyClone China Ltd) and 20 ng/mL macrophage colony-stimulating factor (PeproTech, London, United Kingdom). The cells were incubated at 37 °C in a 5% CO_2 atmosphere (Sanyo). The medium was replaced with fresh cultures and macrophage colony-stimulating factor was added as previously described on day 3. On day 6, different concentrations of TJ-5 (10 and 30 μM) were added 2 h before stimulation with LPS (500 ng/mL, Sigma-Aldrich). Six hours later, the cells were stimulated with ATP (5 mmol/L; InvivoGen, San Diego, CA). After incubation for 2 h, cell culture supernatants and BMDMs were obtained for subsequent assays.

Isolation of Murine Liver Kupffer Cells

Mouse livers were perfused in situ using collagenase (Sigma-Aldrich, Shanghai, China) to create a cell suspension, followed by enrichment of phagocytes by low-speed and gradient centrifugation.[24] Hepatic Kupffer cells were isolated using F4/80 microbeads (MACS, Miltenyi).

Flow Cytometry Analysis and Cell Viability Assay

BMDMs were treated with LPS, ATP, and TJ-5. The cells were then incubated with fluorescein isothiocyanate-conjugated CD11b and phycoerythrin-conjugated F4/80 antibodies (BioLegend, San Diego, CA) at 4 °C for 30 min (protected from light). CD11b expression was detected and analyzed using flow cytometry (BD FACSCalibur platform). For quantification of cell death quantification, BMDMs were harvested for further staining with propidium iodide (PI) for 10 min at room temperature in the dark. The cells were analyzed by flow cytometry (PerCP-Cy5-5 channel). Cell viability was evaluated using a Cell Counting Kit-8 kit (Sigma-Aldrich, Shanghai, China) to determine the appropriate concentrations of TJ-5. BMDMs were seeded into 96-well plates (1×10^5 cells/well) and treated with a concentration gradient of TJ-5. The cells were incubated for 24 h at 37 °C in a 5% CO_2 incubator. Following incubation with Cell Counting Kit-8 reagent for 2 h, the absorbance was measured at 450 nm.

Quantitative Real-time PCR

RNA extraction from liver tissues and BMDM was performed using RNAiso Plus (Takara, Japan) and reverse-transcribed into complementary DNA using the HiScript II Q RT SuperMix Kit (Vazyme, Nanjing, China), according to the manufacturer's instructions. Real-time polymerase chain reaction was performed on a Step One System (Life Technologies) using SYBR qPCR Master Mix (Vazyme, Nanjing, China). Real-time polymerase chain reaction was performed in triplicate and the ΔΔCT method was used to analyze all samples. The primer sequences used for the detection of mouse genes are shown in **Table S1** (**SDC**, http://links.lww.com/TP/C541).

Western Blot Analysis

Total, cytosolic, and nuclear proteins were extracted from tissues or cell samples using a total protein extraction kit and a nuclear/cytoplasmic extraction kit (Beyotime, China). Western blot analysis was performed as previously described, with some modifications.[25] Proteins were separated by SDS-PAGE and transferred onto polyvinylidene fluoride membranes, which were blocked in 5% nonfat milk for 2 h at 37 °C and incubated in the presence of primary antibodies (1:1000 dilution) overnight at 4 °C. The following day, the membranes were washed 4 times with 1× Tris-buffered saline containing 0.5% Tween-20 and incubated with secondary antibodies for 4 h at 4 °C. Finally, all membranes were washed 4 times, after which the blots were visualized using enhanced chemiluminescence (Beyotime). Total protein was used to determine TLR4, MyD88, RAGE, NLRP3, GSDMD/GSDMD-N, caspase-1/cleaved caspase-1, and caspase-11/cleaved caspase-11 expressions (ABclonal Technology Co, Ltd, Wuhan, China). The expression of the NF-κB/P65 (CST, Inc, MA) subunit was measured in cytosolic and nuclear proteins. The Image-Pro Plus software (version 6.0) was used for protein band quantification.

Statistical Analysis

Data are presented as the mean ± SD. Comparisons of means among groups were performed using 1-way ANOVA followed by Dunnett's test when equal variances were assumed. The Brown-Forsythe test was used when equal variance was not assumed. GraphPad Prism 8.0 was used for data analysis. The threshold for statistical significance was set at $P \leq 0.05$.

RESULTS

Inhibition of MyD88 Dimerization Extenuates Liver Injury Following Induction of Hepatic IRI in Mice

We analyzed samples derived from wild-type mice that received a daily intra-abdominal injection of TJ-5 (25, 50, or 75 mg/kg) for 3 successive days and found that TJ-5 at the aforementioned concentrations was safe. These dosages were subsequently used for intra-abdominal injection (Figure 1A). The results showed that mice from the IRI + TJ-5 group, which were intraperitoneally administered 50 mg/kg TJ-5, exhibited significantly improved liver function compared with the IRI group (Figure 1B). Notably, a high number of hepatocytes displayed severe vacuolar degeneration, vascular congestion, and necrotic changes in the IRI group (Figure 1C). TJ-5 also significantly suppressed liver injury to a large extent, as evidenced by a decrease in liver injury scores (Suzuki's score criteria,[22] Figure 1D). Additionally, immunohistochemical staining for MPO showed that TJ-5 remarkably decreased hepatic neutrophil infiltration following hepatic IRI (Figure 1E and F). The latest study indicated that Hepatic IRI could also be alleviated by blocking TLR4 of neutrophils,[26] which may be a new research direction. We found that TJ-5 protected hepatocytes from apoptosis caused by hepatic IRI using the

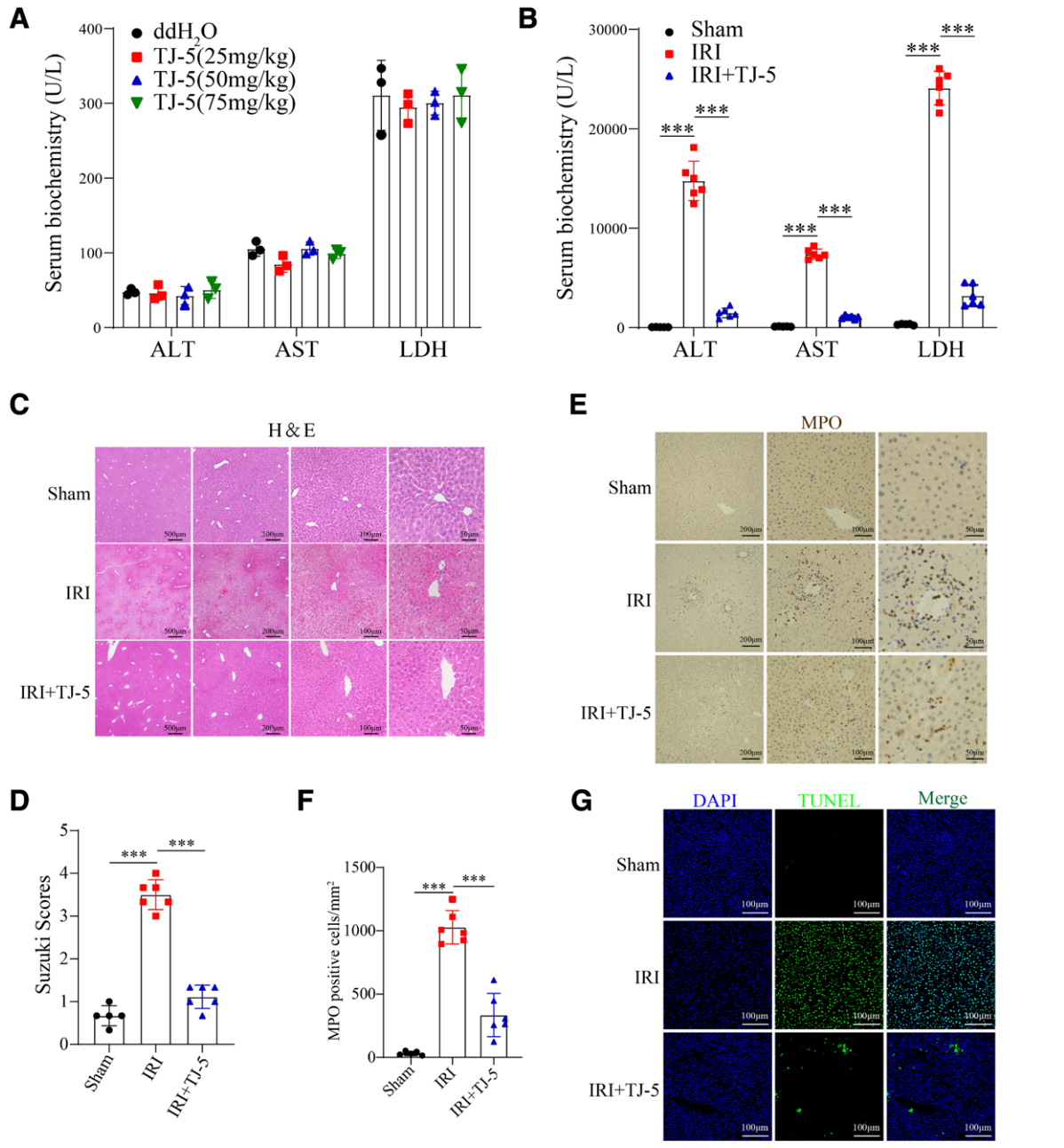

FIGURE 1. Inhibition of MyD88 dimerization extenuates hepatic IRI-induced liver injury in mice. A, The effects of various concentrations of TJ-5 (25, 50, and 75 mg/kg) on liver function of normal wild-type mice. Blood samples were collected from following a single intraperitoneal injection of TJ-5 for 3 consecutive days. Blood samples were also collected from mice not administered with TJ-5. B, Serology tests of liver enzymes in all groups. The IRI + TJ-5 group had significantly lower serum levels of the indicated enzymes compared with the IRI/Sham group. C, Histopathological examination (H&E) of the liver sections in all groups; representative sections are shown. D, The severity of pathological liver injury based on Suzuki's scores. E, Immunohistochemical staining images showing MPO-positive cells in liver tissues. Representative staining images are shown. F, A bar graph displaying the quantitative results of MPO-positive cells/mm^2 per group. G, The TUNEL assay and DAPI staining results illustrating hepatocyte apoptosis levels in each group. Data are expressed as mean ± SD (n = 3~6, per group). ***P < 0.001. Data shown are representative of 3 replicate experiments. ALT, alanine transaminase; AST, aspartate aminotransferase; DAPI, 4',6-diamidino-2-phenylindole; ddH2O, double-distilled water; H&E, hematoxylin and eosin; IRI, ischemia-reperfusion injury; LDH, lactate dehydrogenase; MPO, myeloperoxidase; MyD88, myeloid differentiation factor 88; TJ-5, TJ-M2010-5; TUNEL, terminal deoxynucleotidyltransferase-mediated dUTP nick-end labeling.

terminal deoxynucleotidyltransferase-mediated dUTP nick-end labeling staining assay (Figure 1G). For clinical translation, administration of medication (here TJ-5) >3 d before transplantation is difficult, particularly in donation after circulatory death donors. Therefore, we administered TJ-5 (50 mg/kg) 2 h and 5 min (called preoperative immediate administration) before hepatic ischemia. The results showed that TJ-5 suppressed liver injury as evidenced by a decrease in liver enzymes and liver injury scores in the case of preoperative immediate administration (**Figure S1, SDC,** http://links.lww.com/TP/C541). However, preoperative immediate administration was not as effective as preventive administration for 3 consecutive days. Taken together, these results indicated that TJ-5 not only improves liver function but also

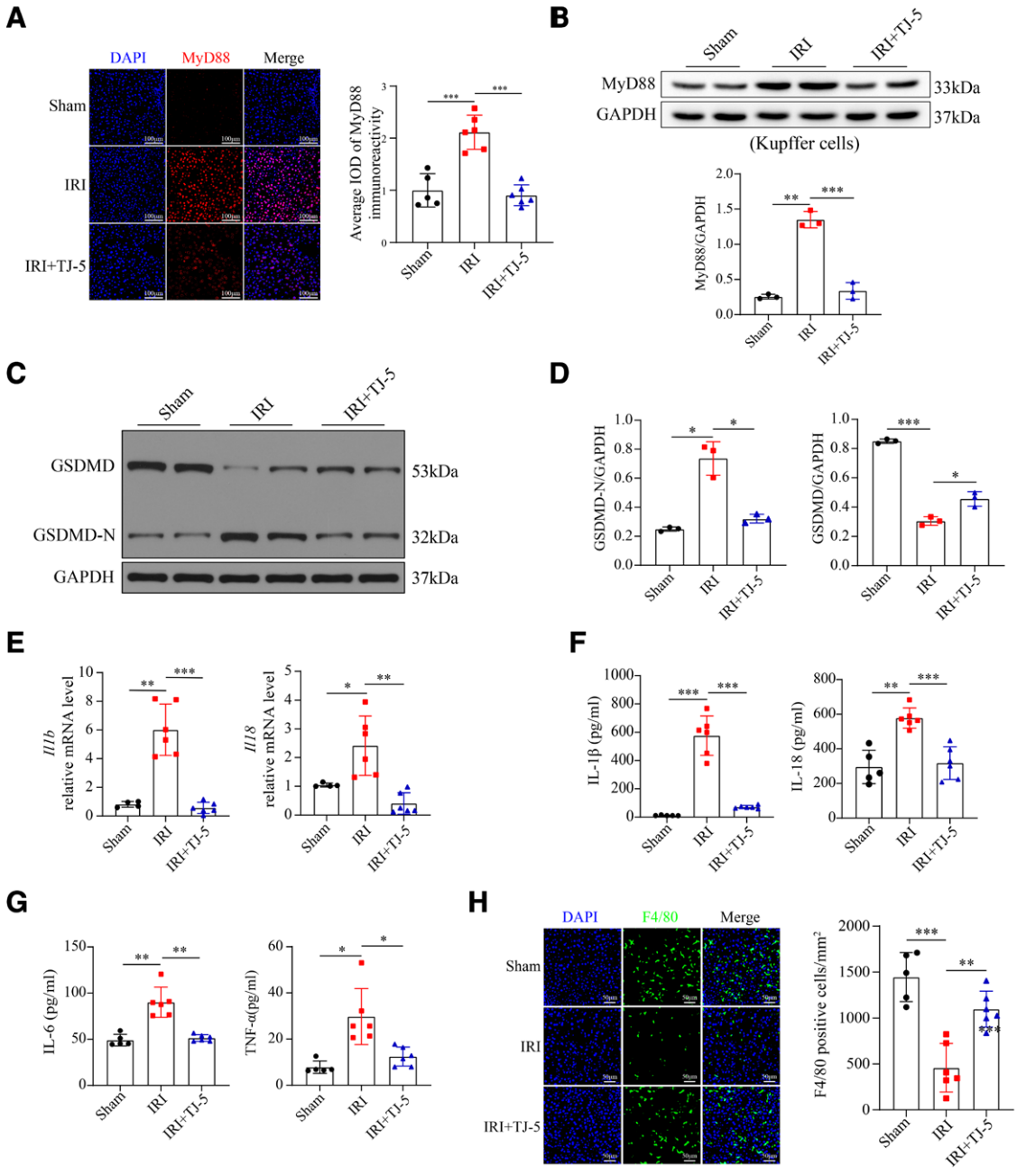

FIGURE 2. TJ-5 suppresses pyroptosis and reduces the secretion of pro-inflammatory factors in mice models of hepatic IRI. A, Staining results of MyD88 (red) and DAPI (blue) in liver tissues. Average IOD values of MyD88 are shown. B, The MyD88 expression level in Kupffer cells in each group. C, Western blotting analysis showing proteins levels of GSDMD and cleaved GSDMD (GSDMD-N) in liver tissues. D, Quantification of Western blot results of GSDMD and GSDMD-N. E, RT-PCR analysis of mRNA expression levels of *Il1b* and *Il18* mRNA in liver tissues. F and G, Levels of serum inflammatory factors as determined by ELISA. H, The representative immunofluorescence images of stained liver sections with F4/80-specific antibody and DAPI indicating the number of macrophages. Quantitative analysis of the number of F4/80-positive cells/mm^2. Data results are expressed as mean ± SD (n = 3~6, each group). $^*P < 0.05$, $^{**}P < 0.01$, and $^{***}P < 0.001$. All data are representative of 3 replicates experiments. ELISA, enzyme-linked immunoassay; DAPI, 4′,6-diamidino-2-phenylindole; GAPDH, glyceraldehyde-3-phosphate dehydrogenase; GSDMD, gasdermin D; IL, interleukin; IOD, integral optical density; IRI, ischemia-reperfusion injury; mRNA, messenger RNA; MyD88, myeloid differentiation factor 88; RT-PCR, real-time polymerase chain reaction; TJ-5, TJ-M2010-5; TNF-α, tumor necrosis factor-α.

attenuates hepatocellular injury and inflammation in mouse hepatic IRI.

TJ-5 Suppresses Pyroptosis During Hepatic IRI and Reduces the Secretion of Pro-inflammatory Factors Induced by Hepatic IRI

IF staining revealed that TJ-5 inhibited the upregulation of MyD88 protein expression in the mouse liver tissues of the IRI group (Figure 2A). The low MyD88 expression observed in the IRI + TJ-5 group may be due to a reduction in the number of immune cells recruited in the liver. To clarify the changes in MyD88 expression in hepatic macrophages, we sorted Kupffer cells from the liver tissues of mice using magnetic beads and found that TJ-5 inhibited MyD88 protein upregulation in the IRI group (Figure 2B). Next, we performed Western

blotting to analyze the expression levels of GSDMD and GSDMD-N in liver tissues and found that GSDMD was cleaved to produce more GSDMD-N following hepatic IRI (Figure 2C). Interestingly, TJ-5 effectively inhibited GSDMD cleavage (Figure 2C and D). Moreover, the TJ-5 also inhibited GSDMD cleavage of Kupffer cells, which were purified from liver tissues (**Figure S2, SDC**, http://links.lww.com/TP/C541). We analyzed the relative messenger RNA expression of pyroptosis-specific inflammatory factors, namely IL-1β and IL-18, in mouse liver tissues and serum samples from each group. The results showed that TJ-5 not only reduced the secretion of pyroptosis-specific inflammatory factors but also downregulated the expression of IL-1β and IL-18 (Figure 2E and F). These results suggest that TJ-5 suppressed pyroptosis in the IRI group.

Additionally, pretreatment of mice with TJ-5 resulted in a significant downregulation in the expression of other pro-inflammatory factors, such as IL-6 and tumor necrosis factor-α, relative to those observed in mice with IRI (Figure 2G). Moreover, hepatic IRI caused a significant reduction in the number of F4/80$^+$ Kupffer cells, indicating that the number of nonviable Kupffer cells was markedly different from that observed in other liver injury models (Figure 2H). This may be attributed to the depletion of hepatic macrophages caused by the induction of pyroptosis on hepatic macrophages.[27] Notably, the TJ-5 treatment effectively reversed this change. Meanwhile, immunohistochemical staining of CD11b$^+$ hepatic monocytes that had been derived from the bone marrow showed that TJ-5 significantly decreased CD11b$^+$ hepatic monocytes infiltration following hepatic IRI (**Figure S3, SDC**, http://links.lww.com/TP/C541). It was also deduced that TJ-5 had a significant inhibitory effect on the induction of pyroptosis in the hepatic tissue and the secretion of pro-inflammatory factors following the induction of hepatic IRI.

TJ-5 May Suppress Pyroptosis by Downregulating the TLR4/MyD88/NF-κB Signaling Pathway in Mice With Hepatic IRI

As expected, TJ-5 markedly inhibited ischemia-reperfusion–induced upregulation of TLR4 and MyD88 expression (Figure 3A–C). Previous studies have reported that the expression and activation of NLRP3 are dependent on the activation of NF-κB.[28] Based on these studies, we determined the levels of nuclear and cytosolic NF-κB/p65 proteins and found that the levels of cytoplasmic NF-κB were decreased, whereas those of nuclear NF-κB were increased in the IRI group (Figure 3D, G). Moreover, the nuclear translocation of NF-κB markedly increased following IRI. Conversely, TJ-5 significantly suppressed NF-κB translocation (Figure 3D, G). Subsequently, we examined the protein levels of NLRP3 and the cleavage of caspase-1 and found that both were markedly upregulated, whereas those of pro-caspase-1 were downregulated following IRI. However, this trend was reversed following TJ-5 treatment (Figure 3E, H, I). Collectively, these results indicate that TJ-5 effectively suppressed canonical pyroptosis by downregulating the TLR4/MyD88/NF-κB signaling pathway.

Furthermore, we focused on the noncanonical pyroptosis pathway and found that TJ-5 effectively inhibited the cleavage of caspase-11 caused by ischemia-reperfusion (Figure 3F, J). These results suggest that TJ-5 suppresses induction of the noncanonical pyroptosis pathway in hepatic IRI. The underlying mechanism of action may entail the regulation of the TLR4/MyD88/NF-κB signaling pathway, although this needs to be experimentally investigated.

TJ-5 Attenuates Pyroptosis in BMDMs Induced by LPS and ATP

BMDM purity was higher than 96% (Figure 4A), and the subsequent results indicated that TJ-5 at a concentration higher than 50 μM exerted significant cytotoxicity on BMDMs (Figure 4B). Consequently, we selected 2 TJ-5 concentrations (10 and 30 μM) for subsequent treatment of BMDMs. In vitro experiments were used to assess the mechanism of hepatic IRI inflammation in LPS-treated macrophages, which simulated the inflammatory process in hepatic IRI.[29-31] The ATP aids in activating the NLRP3 inflammasome in macrophages primed with LPS, thereby causing caspase-1 cleavage and caspase-1-mediated pyroptosis.[32,33]

The results from PI staining and detection of LDH levels did not increase the rate of cell death after a single LPS stimulation, although it markedly increased following combined stimulation by LPS and ATP. Notably, TJ-5 effectively suppressed BMDM cell death induced by LPS and ATP (Figure 4C and D). Moreover, expression analysis revealed that GSDMD was cleaved into GSDMD-N in LPS- and ATP-treated BMDMs. However, TJ-5 effectively inhibited GSDMD cleavage (Figure 4E and F). The results indicated that BMDMs stimulated with a combination of LPS and ATP exhibited slightly higher expression and release of multiple inflammatory factors than those not stimulated. However, TJ-5 suppressed the expression and release of these inflammatory factors in BMDMs in a dose-dependent manner (Figure 5A–D). Taken together, these results indicate that TJ-5 inhibits pyroptosis induced by LPS and ATP in BMDMs.

TJ-5 Reduces LPS and ATP-induced Canonical Pyroptosis in BMDMs by Downregulating the TLR4/MyD88/NF-κB Signaling Pathway

Having established that TJ-5 reduced pyroptosis in BMDMs treated with ATP and LPS, the levels of the canonical pyroptosis-related proteins were detected by Western blotting (Figure 6A–C). In a cell pyroptosis model induced by LPS and ATP, NLRP3 and cleaved caspase-1 levels were significantly elevated, whereas the expression of pro-caspase-1 was suppressed. Cotreatment with LPS and ATP promoted NLRP3 inflammasome activation and induction of the canonical pyroptosis pathway. These effects were significantly suppressed by TJ-5 treatment (Figure 6A–C). TJ-5 inhibited TLR4 and MyD88 levels and promoted the nuclear translocation of NF-κB in BMDM pyroptosis models (Figure 6D–G). Although the TLR4/MyD88/NF-κB pathway was activated by LPS in the absence of ATP, only reduced amounts of canonical pyroptosis were observed. Therefore, TJ-5 inhibited NLRP3 inflammasome activation by blocking the TLR4/MyD88/NF-κB signaling cascade, which in turn suppressed ATP- and LPS-induced canonical pyroptosis in BMDMs.

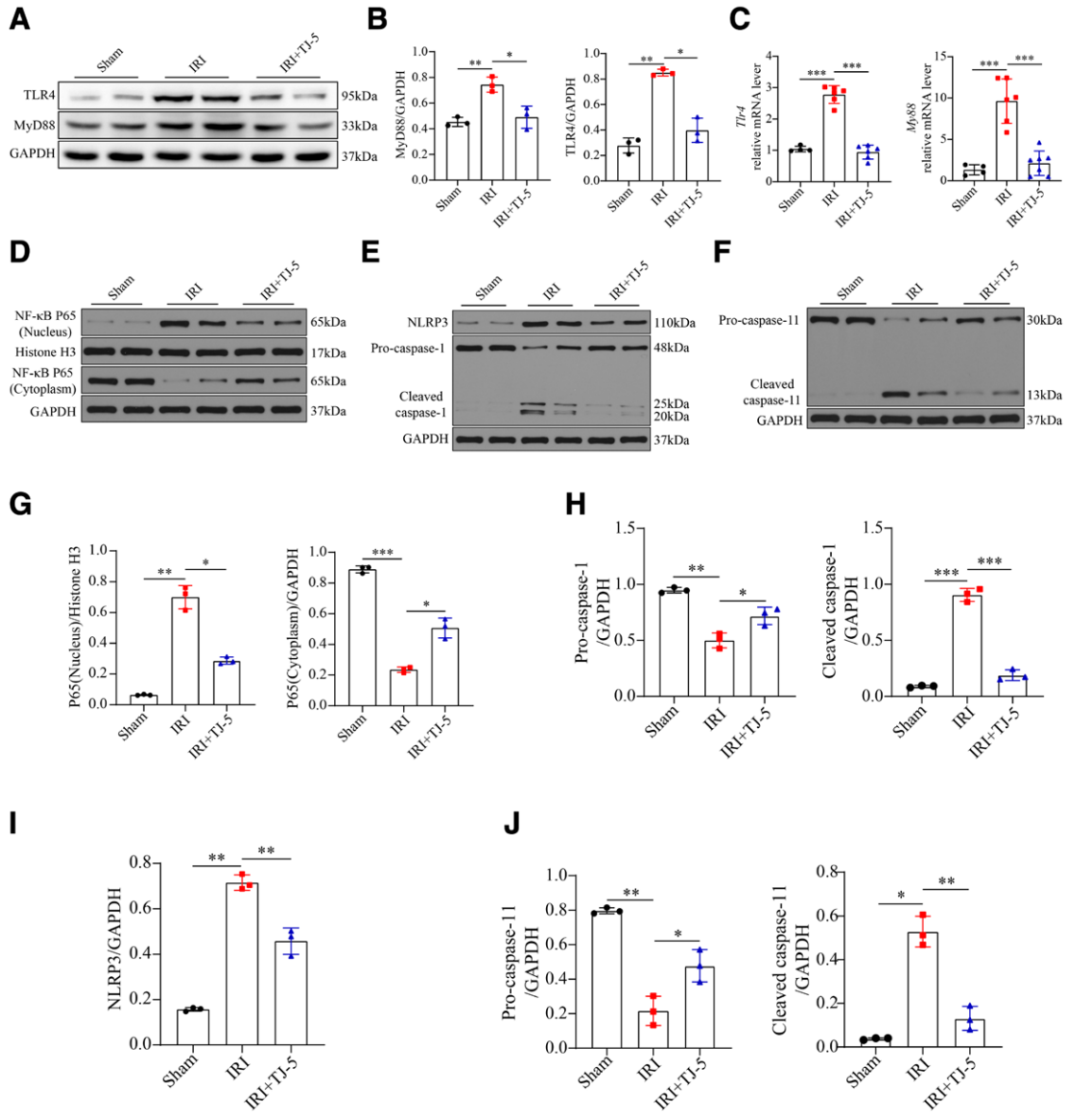

FIGURE 3. TJ-5 may suppress pyroptosis by inhibiting the TLR4/MyD88/NF-κB signaling pathway in mice models of hepatic IRI. A and B, Western blot analysis showing TLR4 and MyD88 expression levels in liver tissues. C, The mRNA expression levels of TLR4 and MyD88 in liver tissue. A histogram showing the relative expression levels. D, Western blotting analysis indicating the expression level of NF-κB p65 in the cytosolic and nuclear domains. E and F, Western blotting results illustrating expression level of NLRP3, pro-caspase-1, cleaved caspase-1, pro-caspase-11, and cleaved caspase-11 in liver tissue samples in the indicated groups. G–J, Quantification of Western blotting bands normalized to proteins bands of GAPDH. Data are expressed as mean ± SD (n = 3~6, each group). *P < 0.05, **P < 0.01, and ***P < 0.001. All data are representative of 3 replicate experiments. GAPDH, glyceraldehyde-3-phosphate dehydrogenase; IRI, ischemia-reperfusion injury; mRNA, messenger RNA; MyD88, myeloid differentiation factor 88; NF-κB, nuclear factor kappa-light-chain-enhancer of activated B cells; TJ-5, TJ-M2010-5; TLR4, Toll-like receptor 4.

TJ-5 May Alleviate Noncanonical Pyroptosis in BMDMs by Inhibiting HMGB1 Secretion and Reducing the Endocytosis of LPS-HMGB1 Complexes

TJ-5 treatment inhibited caspase-11 cleavage, which was initially enhanced by LPS- and ATP-induced cell stimulation (Figure 7A and B). Nonetheless, caspase-11 can directly bind to LPS and induce pyroptosis.[13] This indicated that LPS must cross the plasma membrane to enter the cytoplasm. Extracellular LPS is delivered to the cytoplasm by forming a complex with HMGB1 and activating RAGE signaling. This then induces pyroptosis.[15,34] HMGB1 is translocated from the nucleus to the cytosol in macrophages stimulated with LPS and is secreted into the extracellular region.[35]

HMGB1 forms an LPS-HMGB1 complex with LPS, which enters the cytoplasm via HMGB1/RAGE-mediated endocytosis. To test this hypothesis, HMGB1 levels in supernatants were measured. Stimulation of BMDMs with LPS and ATP promoted HMGB1 secretion, which was inhibited by TJ-5 treatment (Figure 7C). Elevated HMGB1 levels may be attributed to the activation of the canonical pyroptosis pathway in BMDMs. Moreover, TJ-5 inhibited the LPS- and ATP-induced elevation of RAGE expression (Figure 7D and E). To determine the presence of LPS in the cytoplasm after HMGB1-LPS complex endocytosis, BMDMs were treated with LPS-fluorescein isothiocyanate (green) and ATP, with or without TJ-5. The localization of HMGB1 (red) and LPS was determined using IF analysis. Because Triton X-100

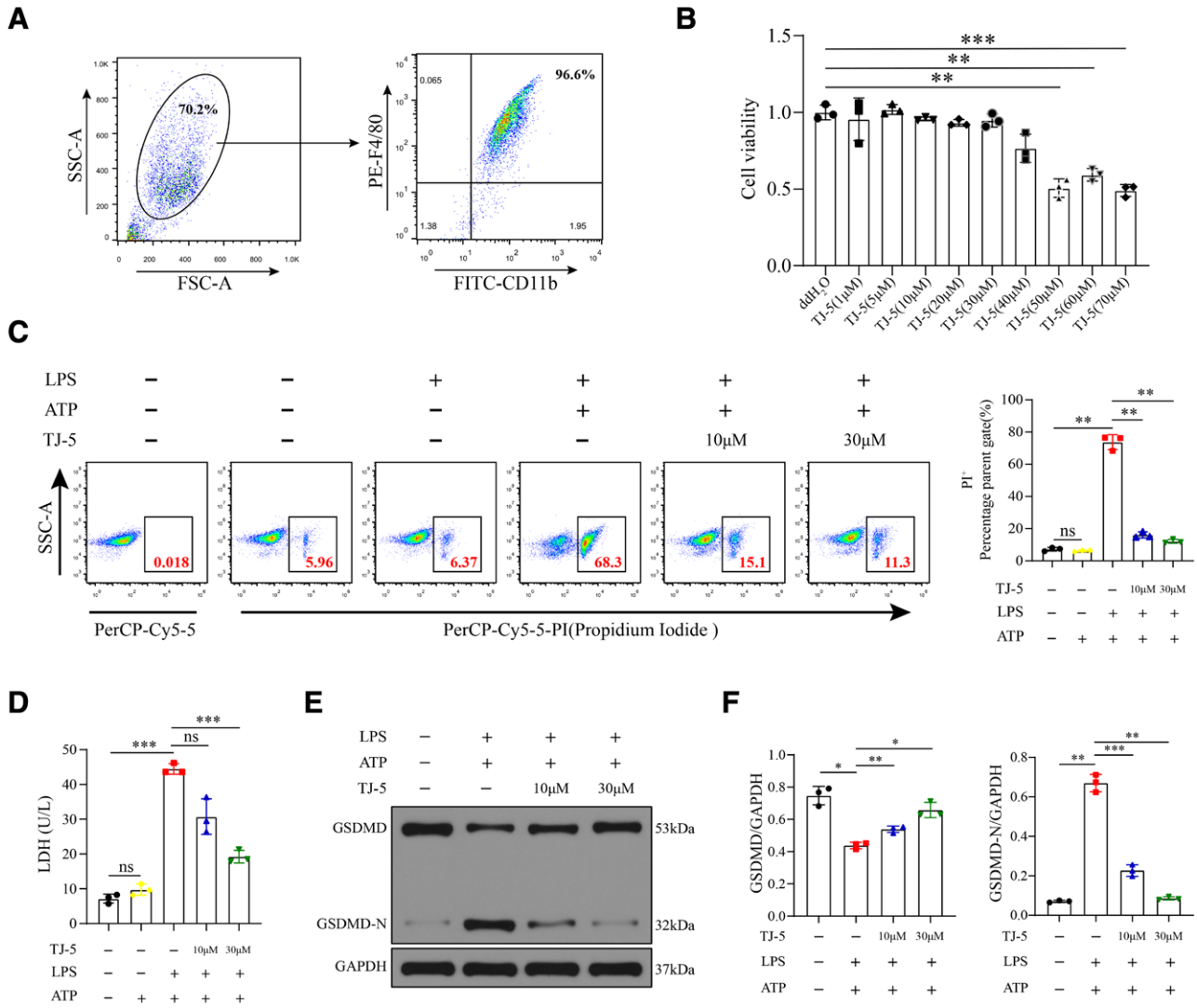

FIGURE 4. TJ-5 attenuates LPS- and ATP-induced pyroptosis of BMDMs. The cells and cell culture supernatants were collected 2 h following ATP treatment. A, Flow cytometry analysis was performed to determine the purity of the BMDM population-based on CD11b and F4/80 antibodies. B, The effects of various concentrations of TJ-5 (1–70 μM) on BMDM viability as determined by the CCK8 assay. C, The PI staining illustrating the proportion of nonviable/dying cells per group; representative results are shown. D, The LDH levels in cell culture supernatants of BMDMs were quantified by an automatic biochemical analyzer. E, Western blotting analysis showing protein expression levels of GSDMD and GSDMD-N in BMDMs in all groups. F, Quantification of Western blot results of GSDMD and GSDMD-N. Data are expressed as mean ± SD (n = 3 samples each group). *$P < 0.05$, **$P < 0.01$, and ***$P < 0.001$. All results are from at least 3 independent repeat experiments. ATP, adenosine triphosphate; ddH2O, double-distilled water; ddH_{2O}, double-distilled water; BMDM, treated bone marrow-derived macrophage; CCK8, Cell Counting Kit-8; FITC, fluorescein isothiocyanate; FSC-A, forward-scatter area; GAPDH, glyceraldehyde-3-phosphate dehydrogenase; GSDMD, gasdermin D; LDH, lactate dehydrogenase; LPS, lipopolysaccharide; ns, not significant; PE, phycoerythrin; PI, propidium iodide; SSC-A, side scatter area; TJ-5, TJ-M2010-5.

enhances nuclear membrane permeability, IF staining was performed without Triton X-100 to determine cytosolic HMGB1 expression. Nuclear staining was performed using Hoechst (blue), which can penetrate the nuclear membrane efficiently. LPS colocalized with HMGB1 in the cytoplasm, and large amounts of LPS and HMGB1 were observed in the cytoplasm of BMDMs following LPS and ATP exposure (Figure 7F). The average Manders coefficient was 0.999 ± 0, whereas the average Pearson coefficient was 0.596 ± 0.035 (mean ± SD, n = 4). Intracellular LPS and HMGB1 levels were markedly suppressed in BMDMs pretreated with TJ-5. To verify whether the HMGB1-LPS complex was transported into cells via HMGB1-dependent endocytosis, BMDMs were treated with LPS and HMGB1 for 8 h with or without prestimulation with TJ-5. LPS was found to be colocalized with HMGB1 in the cytoplasm, with an average Manders coefficient of 0.785 ± 0.049, whereas the average Pearson coefficient was 0.661 ± 0.06 (mean ± SD, n = 3) (Figure 7F). LPS did not enter the cytosol of BMDMs treated with LPS alone. However, LPS and HMGB1 were both transported in bulk into the cytoplasm of BMDMs treated with LPS and HMGB1. TJ-5 blocked the entry of LPS and HMGB1 into the cytoplasm (Figure 7G).

These findings imply that TJ-5 inhibits HMGB1 secretion and prevents LPS-HMGB1 complexes from entering the cytoplasm in LPS-HMGB1–induced pyroptosis models, which in turn alleviates the noncanonical pyroptosis pathway.

DISCUSSION

Previous studies have shown that the TLR4/MyD88 signaling pathway is closely related to hepatic IRI.[5,36,37] In the present study, we found that TJ-5, a novel

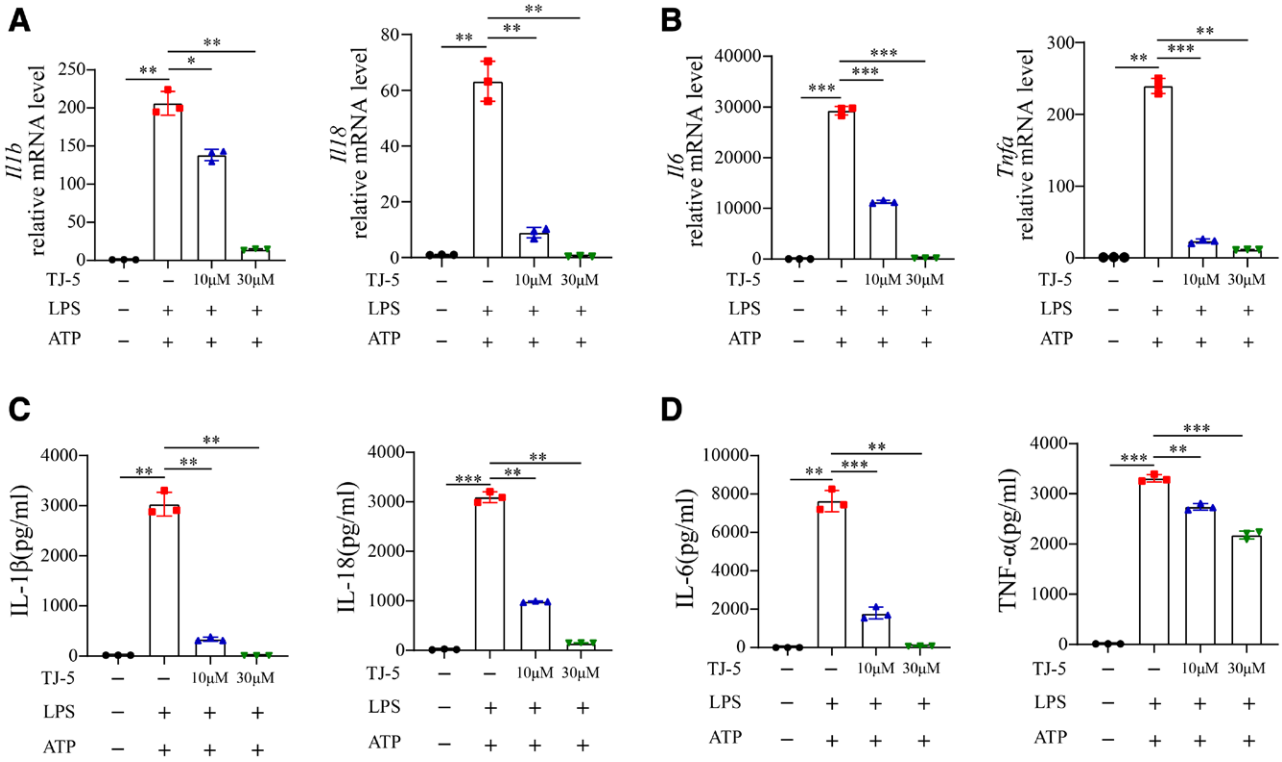

FIGURE 5. Inhibition of MyD88 reduces the secretion of inflammatory factors in BMDMs treated with LPS and ATP. A and B, The real-time PCR results showing mRNA levels of *Il1b*, *Il18*, *Il6*, and *Tnfa* in BMDMs. C and D, The expression level of specific inflammatory cytokines (IL-1β, IL-18, IL-6, and TNF-α) in cell culture supernatants of BMDMs based on ELISA. A histogram showing summarized results. Data are expressed as mean ± SD (n = 3 samples each group). $^{*}P < 0.05$, $^{**}P < 0.01$, and $^{***}P < 0.001$. All the experimental results shown in the Figures are from at least 3 independent repeat experiments. BMDM, bone marrow-derived macrophage; ELISA, enzyme-linked immunoassay; IL, interleukin; LPS, lipopolysaccharide; mRNA, messenger RNA; MyD88, myeloid differentiation factor 88; PCR, polymerase chain reaction; TNF-α, tumor necrosis factor-α.

MyD88 inhibitor, exerted satisfactory protective effects by reducing the extent of liver IRI. Previous studies have mainly focused on the role of the TLR4/MyD88 signaling pathway in hepatic IRI.[4,5,36,37] In the present study, we observed GSDMD cleavage during hepatic IRI, suggesting that pyroptosis may be involved in hepatic IRI. Moreover, TJ-5 inhibited pyroptosis during hepatic IRI, suggesting that the TLR4/MyD88 signaling pathway plays a key role in the induction of pyroptosis in hepatic IRI.

Pyroptosis was initially reported to occur in immune cells[38] but not in hepatocytes during hepatic IRI.[6] To date, 2 main pyroptosis signaling pathways, namely caspase-1-dependent canonical[39] and caspase-11-dependent noncanonical,[40] have been reported. Interestingly, the cleavage of caspase-1 and caspase-11 was significantly upregulated in the mouse hepatic IRI model, suggesting that both canonical and noncanonical pyroptosis signaling pathways were activated. Additionally, we detected F4/80^{+} Kupffer cell depletion during hepatic IRI, which is consistent with the findings of a previous study.[27] Notably, MyD88 inhibitors not only reduced the activation of both canonical and noncanonical pyroptosis pathways but also significantly improved Kupffer cell depletion in liver tissues during hepatic IRI. Additionally, TJ-5 effectively inhibited the nuclear translocation of NF-κB and expression levels of TLR4, MyD88, and NLRP3. Based on these findings, we inferred that TJ-5 suppresses hepatic IRI-induced canonical pyroptosis by downregulating the TLR4/MyD88/NF-κB signaling pathway. Although TJ-5 suppresses noncanonical pyroptosis in hepatic IRI, the underlying mechanism remains unclear, necessitating further research.

Next, we elucidated the mechanism underlying in vitro inhibitory effect of TJ-5 on the noncanonical pyroptosis signaling pathway. To this end, we established an in vitro pyroptosis model following the stimulation of BMDMs with LPS and ATP.[41] As expected, the results of in vitro experiments corroborated those of in vivo assay. TJ-5 inhibits caspase-1-dependent canonical pyroptosis and caspase-11-dependent noncanonical pyroptosis induced by LPS and ATP. It inhibits the activation of the canonical NLRP3 inflammasome by downregulating the TLR4/MyD88/NF-κB signaling pathway and reducing the cleavage of caspase-1, which in turn alleviates canonical pyroptosis. A recent study reported that pyroptosis-induced cell lysis is sufficient for the release of HMGB1 into the extracellular space.[35] Extracellular LPS-HMGB1 complexes bind to RAGE expressed on the cell surface-expressed RAGE and are endocytosed in the cytoplasm. Subsequently, LPS binds to its key pathogenic cytosolic receptor, caspase-11, to mediate noncanonical pyroptosis (Figure 8).[42,43] Our work has shown that TJ-5 may suppress HMGB1 release not only by inhibiting canonical pyroptosis, but also by inhibiting the upregulation of RAGE expression in cells treated with LPS and ATP. The results of the present study revealed that TJ-5 might prevent endocytosis of LPS-HMGB1 complexes caused by LPS and ATP, as well as LPS and HMGB1, thereby

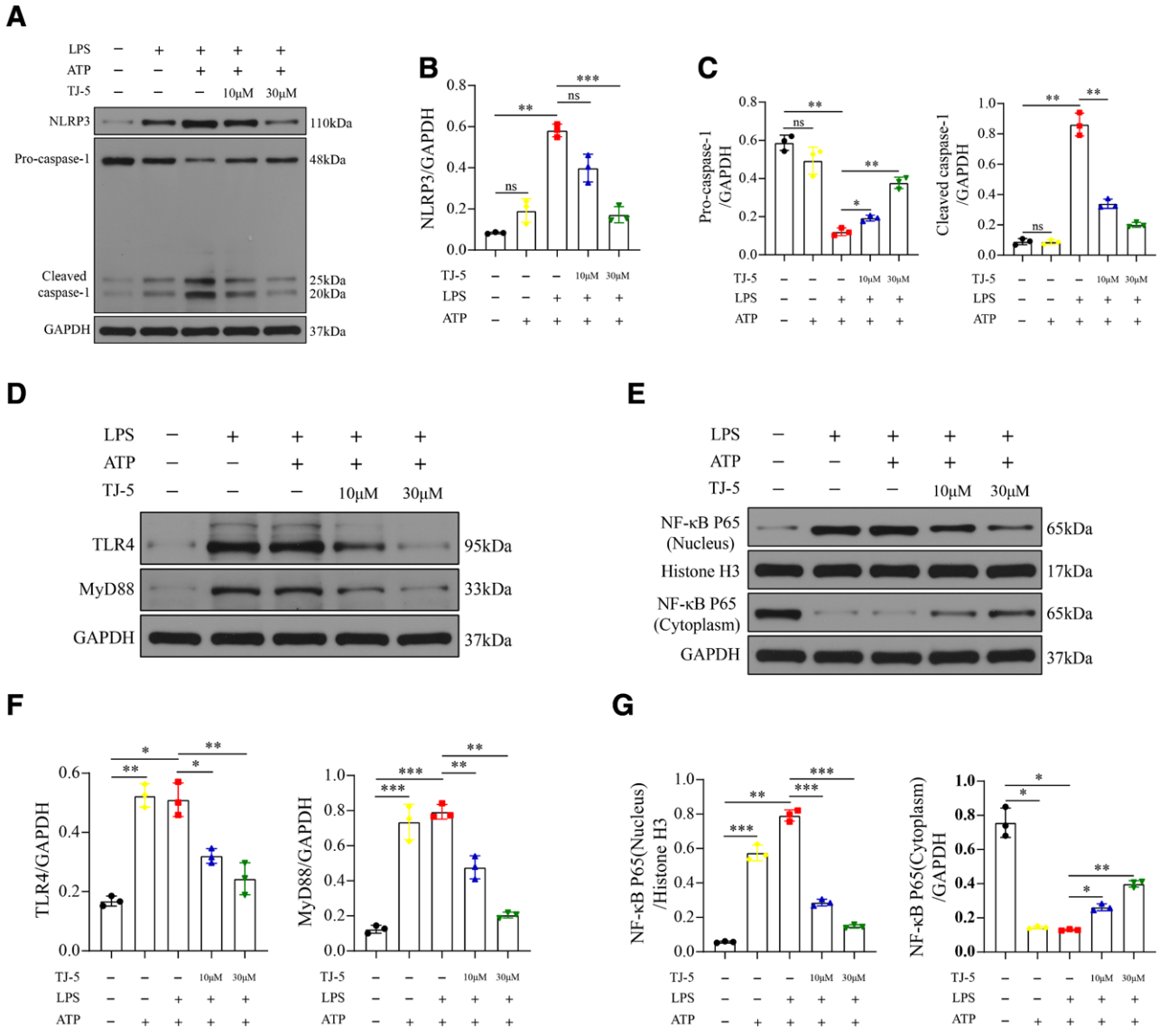

FIGURE 6. TJ-5 reduces LPS- and ATP-induced canonical pyroptosis in BMDMs by suppressing the TLR4/MyD88/NF-κB signaling pathway. A and D, Western blotting results showing protein levels of NLRP3, pro-caspase-1, cleaved caspase-1, TLR4, and MyD88 in BMDMs. E, Western blotting analysis indicating the expression levels of NF-κB p65 in cytosolic and nuclear domains of BMDMs. B, C, F, and G, A histogram showing Western blot bands. Data are expressed as mean ± SD (n=3 samples each group). *$P < 0.05$, **$P < 0.01$, and ***$P < 0.001$. Each independent experiment included 3 replicates. BMDM, bone marrow-derived macrophage; GAPDH, glyceraldehyde-3-phosphate dehydrogenase; LPS, lipopolysaccharide; MyD88, myeloid differentiation factor 88; NF-κB, nuclear factor kappa-light-chain-enhancer of activated B cells; NLRP3, nucleotide-binding oligomerization domain-like receptors family pyrin domain containing 3; TJ-5, TJ-M2010-5; TLR4, Toll-like receptor 4.

inhibiting the noncanonical pyroptosis pathway. This phenomenon is most likely caused by TJ-5's action in inhibiting activation of the HMGB1/RAGE signaling pathway. HMGB1 can also mediate caspase-11-dependent pyroptosis.[15] This explains the occurrence of noncanonical pyroptosis during hepatic IRI and why TJ-5 effectively inhibits both the canonical and noncanonical pyroptosis pathways.

The following interesting findings were noted in the present study: (1) the MyD88 inhibitor TJ-5 significantly ameliorated liver injury during hepatic IRI; (2) TJ-5 effectively inhibited pyroptosis and hepatic macrophage depletion in a mouse hepatic IRI model; and (3) TJ-5 alleviated canonical pyroptosis in BMDMs by downregulating the TLR4/MyD88/NF-κB signaling pathway, as well as noncanonical pyroptosis in BMDMs by inhibiting HMGB1 release and suppressing endocytosis of LPS-HMGB1 complexes (Figure 8). In summary, TJ-5 protected against hepatic IRI by suppressing pyroptosis, a phenomenon that may be due to the inhibition of liver inflammatory immune activation. The drug candidate identified in this study not only significantly protected the liver against IRI but also concomitantly inhibited both canonical and noncanonical pyroptosis signaling pathways. This evidence provides novel directions to guide future efforts to explore the inflammatory mechanisms underlying hepatic IRI and cellular pyroptosis.

However, the present study has some limitations. First, we did not explore in-depth the types of

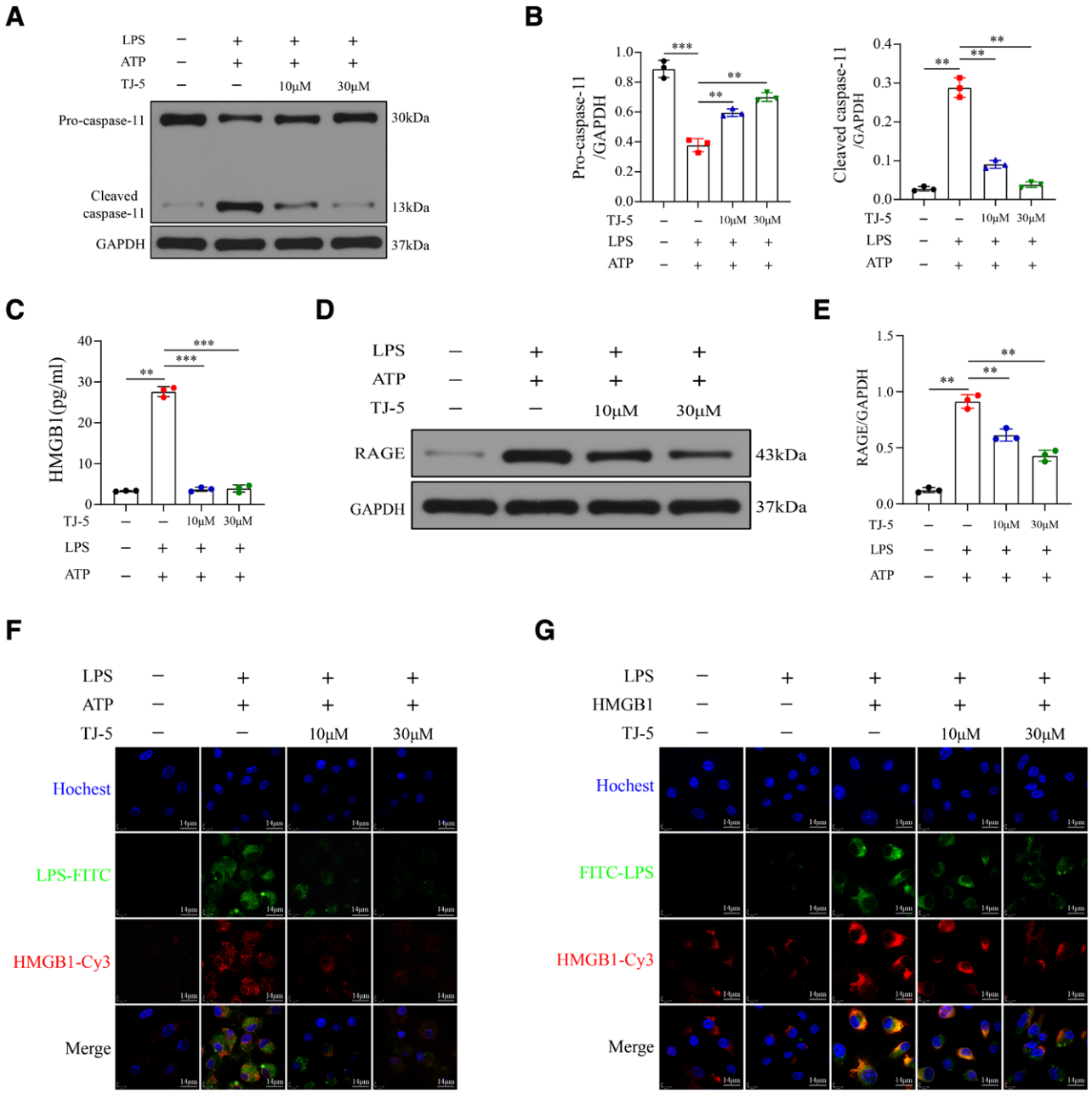

FIGURE 7. TJ-5 may alleviate noncanonical pyroptosis in BMDMs by inhibiting HMGB1 secretion and reducing endocytosis of LPS-HMGB1 complexes. A and B, Western blotting results showing protein expression levels of pro-caspase-11 and cleaved caspase-11. C, The expression level of HMGB1 in cell culture supernatants of BMDMs as determined by ELISA. D and E, Western blotting results indicating the protein expression level of RAGE. F, BMDMs were treated with LPS-FITC (green) and ATP with or without TJ-5. Immunofluorescence microscopic images showing cellular localization of HMGB1 (red) and LPS. The nuclear region was stained with Hoechst (blue). Representative confocal immunofluorescence microscopic images are shown. G, BMDMs were pretreated with or without TJ-5 for 2 h and then stimulated with LPS (500 ng/mL) and HMGB1 (400 μg/mL) for 8 h. Immunofluorescence microscopic images showing cellular localization of HMGB1 (red) and LPS; the nuclear region was stained with Hoechst (blue). Representative confocal immunofluorescence microscopic images are shown. Data are expressed as mean ± SD (n = 3 samples each group). $^{*}P < 0.05$, $^{**}P < 0.01$, and $^{***}P < 0.001$. Each independent experiment included 3 replicates. BMDMs, bone marrow-derived macrophages; ELISA, enzyme-linked immunoassay; FITC, fluorescein isothiocyanate; GAPDH, glyceraldehyde-3-phosphate dehydrogenase; HMGB1, high-mobility group box-1; LPS, lipopolysaccharide; RAGE, receptor for advanced glycation end products; TJ-5, TJ-M2010-5.

intrahepatic cells (may hepatic Kupffer cells, **Figure S2, SDC**, http://links.lww.com/TP/C541) that undergo pyroptosis during hepatic IRI. We found that preoperative immediate administration was less effective than preventive administration for 3 consecutive days, which was a limitation to the translation of the drug candidate into the clinic. TJ-5 inhibited MyD88 dimerization by interacting with the MyD88 Toll/interleukin-1–receptor domain. TJ-5 was designed to inhibit MyD88 dimerization. Theoretically, TJ-5 does not affect the expression of MyD88 and its upstream proteins such as TLR4 and RAGE. However, this was also observed in the present study. Certain feedback mechanisms that require further attention may be present.

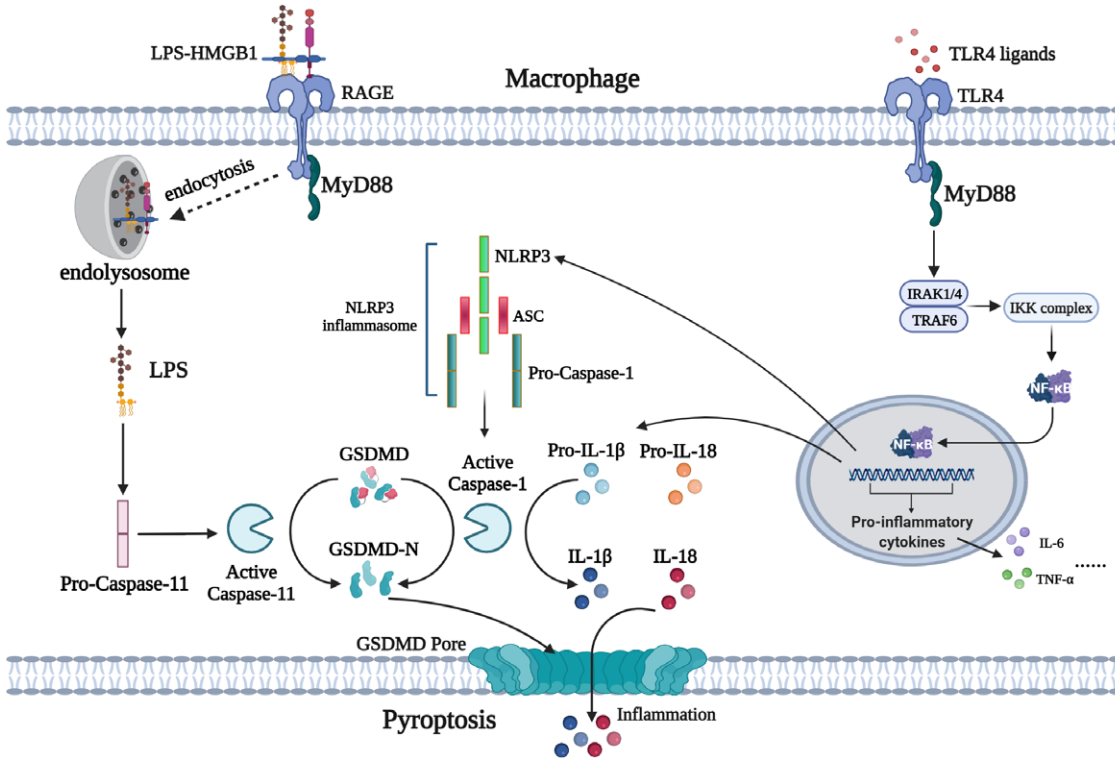

FIGURE 8. A diagram illustrating the potential signaling pathway underlying development of pyroptosis in macrophages. Previous studies have shown that pyroptosis occurs exclusively in myeloid innate immune cells during hepatic IRI. LPS or other endogenous factors activate TLR4/MyD88/NF-κB, which induces the nuclear translocation of NF-κB. The activated NF-κB signaling pathway increases cellular expression of inflammatory cytokines and activation of NLRP3. The activated NLRP3 forms a complex termed NLRP3 inflammasome with ASC and pro-caspase-1. The inflammasome complex transforms pro-caspase-1 into mature form (caspase-1). Activated caspase-1 cleaves pro-IL-1β and pro-IL-18 into active IL-1β and IL-18, respectively, and GSDMD into GSDMD-N, resulting in the induction of pyroptosis because of the formation of pores on the cellular membrane. This process is referred to as canonical pyroptosis. In the present study, results showed that pyroptosis triggered the release of inflammatory cytokines and HMGB1. LPS-HMGB1 complex enters the cytoplasm through the endolysosome pathway stimulating endocytosis. The intracytoplasmic LPS released from the endolysosome directly activates caspase-11, which then cleaves GSDMD into GSDMD-N resulting in occurrence of pyroptosis. This pathway is known as the noncanonical pathway of pyroptosis. The diagram was created using the BioRender website (https://biorender.com/). ASC, apoptosis-associated speck-like protein; GSDMD, gasdermin D; HMGB1, high-mobility group box-1; IL, interleukin; IRI, ischemia-reperfusion injury; LPS, lipopolysaccharide; MyD88, myeloid differentiation factor 88; NF-κB, nuclear factor kappa-light-chain-enhancer of activated B cells; NLRP3, nucleotide-binding oligomerization domain-like receptors family pyrin domain containing 3; RAGE, receptor for advanced glycation end products; TLR4, Toll-like receptor 4; TNF-α, tumor necrosis factor-α.

REFERENCES

1. Zhou J, Hu M, He M, et al. TNFAIP3 interacting protein 3 is an activator of hippo-YAP signaling protecting against hepatic ischemia/reperfusion injury. *Hepatology*. 2021;74:2133–2153.
2. Lu L, Zhou H, Ni M, et al. Innate immune regulations and liver ischemia-reperfusion injury. *Transplantation*. 2016;100:2601–2610.
3. Vasileiou I, Kostopanagiotou G, Katsargyris A, et al. Toll-like receptors: a novel target for therapeutic intervention in intestinal and hepatic ischemia-reperfusion injury? *Expert Opin Ther Targets*. 2010;14:839–853.
4. Huang J, Yue S, Ke B, et al. Nuclear factor erythroid 2-related factor 2 regulates toll-like receptor 4 innate responses in mouse liver ischemia-reperfusion injury through Akt-forkhead box protein O1 signaling network. *Transplantation*. 2014;98:721–728.
5. Koh WU, Kim J, Lee J, et al. Remote ischemic preconditioning and diazoxide protect from hepatic ischemic reperfusion injury by inhibiting HMGB1-induced TLR4/MyD88/NF-κB signaling. *Int J Mol Sci*. 2019;20:E5899.
6. Li J, Zhao J, Xu M, et al. Blocking GSDMD processing in innate immune cells but not in hepatocytes protects hepatic ischemia-reperfusion injury. *Cell Death Dis*. 2020;11:244.
7. Kadono K, Kageyama S, Nakamura K, et al. Myeloid Ikaros-SIRT1 signaling axis regulates hepatic inflammation and pyroptosis in ischemia-stressed mouse and human liver. *J Hepatol*. 2022;76:896–909.
8. Kolachala VL, Lopez C, Shen M, et al. Ischemia reperfusion injury induces pyroptosis and mediates injury in steatotic liver thorough Caspase 1 activation. *Apoptosis*. 2021;26:361–370.
9. Sun P, Zhong J, Liao H, et al. Hepatocytes are resistant to cell death from canonical and non-canonical inflammasome-activated pyroptosis. *Cell Mol Gastroenterol Hepatol*. 2022;13:739–757.
10. Bauernfeind FG, Horvath G, Stutz A, et al. Cutting edge: NF-kappaB activating pattern recognition and cytokine receptors license NLRP3 inflammasome activation by regulating NLRP3 expression. *J Immunol*. 2009;183:787–791.
11. Pang Y, Wu D, Ma Y, et al. Reactive oxygen species trigger NF-κB-mediated NLRP3 inflammasome activation involvement in low-dose CdTe QDs exposure-induced hepatotoxicity. *Redox Biol*. 2021;47:102157.
12. Shi J, Zhao Y, Wang K, et al. Cleavage of GSDMD by inflammatory caspases determines pyroptotic cell death. *Nature*. 2015;526:660–665.
13. Ding J, Shao F. SnapShot: the noncanonical inflammasome. *Cell*. 2017;168:544–544.e1.
14. Guo H, Callaway JB, Ting JP. Inflammasomes: mechanism of action, role in disease, and therapeutics. *Nat Med*. 2015;21:677–687.
15. Kim HM, Kim YM. HMGB1: LPS delivery vehicle for caspase-11-mediated pyroptosis. *Immunity*. 2018;49:582–584.
16. Prantner D, Nallar S, Vogel SN. The role of RAGE in host pathology and crosstalk between RAGE and TLR4 in innate immune signal transduction pathways. *Faseb J*. 2020;34:15659–15674.
17. Xie L, Jiang FC, Zhang LM, et al. Targeting of MyD88 homodimerization by novel synthetic inhibitor TJ-M2010-5 in preventing colitis-associated colorectal cancer. *J Natl Cancer Inst*. 2016;108:djv364.
18. Li C, Zhang LM, Zhang X, et al. Short-term pharmacological inhibition of MyD88 homodimerization by a novel inhibitor promotes

robust allograft tolerance in mouse cardiac and skin transplantation. *Transplantation*. 2017;101:284–293.
19. Ji H, Liu Y, Zhang Y, et al. T-cell immunoglobulin and mucin domain 4 (TIM-4) signaling in innate immune-mediated liver ischemia-reperfusion injury. *Hepatology*. 2014;60:2052–2064.
20. Han Z, Li Y, Yang B, et al. Agmatine attenuates liver ischemia reperfusion injury by activating Wnt/β-catenin signaling in mice. *Transplantation*. 2020;104:1906–1916.
21. Ni M, Fu H, Huang F, et al. Vagus nerve attenuates hepatocyte apoptosis upon ischemia-reperfusion via α7 nicotinic acetylcholine receptor on kupffer cells in mice. *Anesthesiology*. 2016;125:1005–1016.
22. Suzuki S, Toledo-Pereyra LH, Rodriguez FJ, et al. Neutrophil infiltration as an important factor in liver ischemia and reperfusion injury. Modulating effects of FK506 and cyclosporine. *Transplantation*. 1993;55:1265–1272.
23. Zhang P, Zhou X, He M, et al. Ultrasensitive detection of circulating exosomes with a 3D-nanopatterned microfluidic chip. *Nat Biomed Eng*. 2019;3:438–451.
24. Aparicio-Vergara M, Tencerova M, Morgantini C, et al. Isolation of kupffer cells and hepatocytes from a single mouse liver. *Methods Mol Biol*. 2017;1639:161–171.
25. Zou Z, Du D, Miao Y, et al. TJ-M2010-5, a novel MyD88 inhibitor, corrects R848-induced lupus-like immune disorders of B cells in vitro. *Int Immunopharmacol*. 2020;85:106648.
26. Liu Y, Lei Z, Chai H, et al. Thrombomodulin-mediated inhibition of neutrophil extracellular trap formation alleviates hepatic ischemia-reperfusion injury by blocking TLR4 in rats subjected to liver transplantation. *Transplantation*. 2022;106:e126–e140.
27. Hua S, Ma M, Fei X, et al. Glycyrrhizin attenuates hepatic ischemia-reperfusion injury by suppressing HMGB1-dependent GSDMD-mediated kupffer cells pyroptosis. *Int Immunopharmacol*. 2019;68:145–155.
28. He Y, Hara H, Núñez G. Mechanism and regulation of NLRP3 inflammasome activation. *Trends Biochem Sci*. 2016;41:1012–1021.
29. Li CX, Ng KT, Shao Y, et al. The inhibition of aldose reductase attenuates hepatic ischemia-reperfusion injury through reducing inflammatory response. *Ann Surg*. 2014;260:317–328.
30. Xu D, Zhu J, Jeong S, et al. Rictor deficiency aggravates hepatic ischemia/reperfusion injury in mice by suppressing autophagy and regulating MAPK signaling. *Cell Physiol Biochem*. 2018;45:2199–2212.
31. Zhang P, Ming Y, Ye Q, et al. Comprehensive circRNA expression profile during ischemic postconditioning attenuating hepatic ischemia/reperfusion injury. *Sci Rep*. 2019;9:264.
32. Mariathasan S, Weiss DS, Newton K, et al. Cryopyrin activates the inflammasome in response to toxins and ATP. *Nature*. 2006;440:228–232.
33. He WT, Wan H, Hu L, et al. Gasdermin D is an executor of pyroptosis and required for interleukin-1β secretion. *Cell Res*. 2015;25:1285–1298.
34. Yang H, Liu H, Zeng Q, et al. Inhibition of HMGB1/RAGE-mediated endocytosis by HMGB1 antagonist box A, anti-HMGB1 antibodies, and cholinergic agonists suppresses inflammation. *Mol Med*. 2019;25:13.
35. Volchuk A, Ye A, Chi L, et al. Indirect regulation of HMGB1 release by gasdermin D. *Nat Commun*. 2020;11:4561.
36. Du Y, Qian B, Gao L, et al. Aloin preconditioning attenuates hepatic ischemia/reperfusion injury via inhibiting TLR4/MyD88/NF-κB signal pathway in vivo and in vitro. *Oxid Med Cell Longev*. 2019;2019:3765898.
37. Huang HF, Zeng Z, Wang KH, et al. Heme oxygenase-1 protects rat liver against warm ischemia/reperfusion injury via TLR2/TLR4-triggered signaling pathways. *World J Gastroenterol*. 2015;21:2937–2948.
38. Fink SL, Cookson BT. Apoptosis, pyroptosis, and necrosis: mechanistic description of dead and dying eukaryotic cells. *Infect Immun*. 2005;73:1907–1916.
39. Miao EA, Leaf IA, Treuting PM, et al. Caspase-1-induced pyroptosis is an innate immune effector mechanism against intracellular bacteria. *Nat Immunol*. 2010;11:1136–1142.
40. Kayagaki N, Stowe IB, Lee BL, et al. Caspase-11 cleaves gasdermin D for non-canonical inflammasome signalling. *Nature*. 2015;526:666–671.
41. Hu JJ, Liu X, Xia S, et al. FDA-approved disulfiram inhibits pyroptosis by blocking gasdermin D pore formation. *Nat Immunol*. 2020;21:736–745.
42. Deng M, Tang Y, Li W, et al. The endotoxin delivery protein HMGB1 mediates caspase-11-dependent lethality in sepsis. *Immunity*. 2018;49:740–753.e7.
43. Xu J, Jiang Y, Wang J, et al. Macrophage endocytosis of high-mobility group box 1 triggers pyroptosis. *Cell Death Differ*. 2014;21:1229–1239.